RF Interference Mitigation for Dual S-Band Links on a 6U CubeSat: Preliminary Hardware Validation

N. Khorchef[1,*], E. Obreque[1], A. Riaz[1],
E. Scullion[1], R. Wicks[1], , R. Binns[1], J. Vernon[1]
[1] Northumbria University, Newcastle upon Tyne
NE1 8ST, United Kingdom
[*] nassima.khorchef@northumbria.ac.uk

***Abstract*—This paper presents the RF communication system architecture and preliminary hardware validation for the ALIGN (Autonomous Laser-based Inter-satellite Gigabit Network) mission, comprising a pair of 6U CubeSats equipped with FOCUS (Free-space Optical Communications Unit for Space), an experimental payload demonstrating high-data-rate optical inter-satellite links in Low Earth Orbit (LEO). Each platform features co-located S-band Radio Ground-to-Satellite Link (RGSL) and Radio Inter-satellite Link (RISL) subsystems operating within the same frequency band (2025–2110 MHz). The compact CubeSat form factor and SWaP-C constraints impose significant limitations on the achievable isolation between the two RF links, making co-site RFI management a critical design challenge. A multi-layered mitigation strategy is implemented, combining Time Division Multiplexing (TDM) at the protocol level with hardware-level isolation strategies including asymmetric transceiver duplex configuration, 55 MHz frequency separation, orthogonal antenna placement providing 15 cm physical separation and 90 $^\circ$ angular isolation, and polarization diversity between the RHCP RGSL and LP RISL links between antennas. The end-to-end hardware feasibility test was conducted using Flight Model (FM) modules in a certified anechoic chamber under far-field conditions and across the full operational power range of both links, constituting a valid first-step validation approach within the equipment and budget constraints typical of university CubeSat projects. The results confirmed successful preliminary bilateral RISL handshake and the absence of co-site RFI at the RGSL across all tested configurations, validating the combined isolation strategy as an effective and practical approach within the SWaP-C constraints of the platform. These findings provide an initial validated design framework for establishing multi-link RF systems of constellation of CubeSats within the same frequency band.**

***Index Terms*—CubeSat, S-band inter-satellite links, Radio frequency interference, mitigation strategies**

I. Introduction

The landscape of small satellite missions has undergone a remarkable transformation in recent years. CubeSats, once confined to university educational and experiment projects, have evolved into capable platforms now playing critical roles in In-Orbit Demonstration (IOD) and Validation (IOV) missions for leading space agencies such as NASA and ESA, with growing presence in LEO constellations and formation flying configurations. This places them alongside, and increasingly as part of, large-scale commercial satellite mission [1]–[8]. However, this elevated role comes with a corresponding increase in expectations. CubeSats must now satisfy the same operational standards, link performance requirements, and interference management challenges as their larger counterparts, while remaining constrained by the fundamental Size, Weight, Power, and Cost (SWaP-C) limitations inherent to their form factor. This dual pressure, meeting mission-grade technical requirements within tightly bounded hardware constraints, makes the design of CubeSat communication systems increasingly complex and highly competitive. Among many critical challenges in this context is the management of Radio Frequency Interference (RFI), which affects the performance of the RF link of any satellite system regardless of its scale [9]. This requires a rigorous analysis from the early stages of mission design.

RFI refers to any unwanted signal that degrades the quality of a desired communication link. In satellite systems, RFI occurs when transmitted signals from one or more sources overlap in frequency with the intended signal at the receiver. Two primary forms are relevant to co-located RF systems: co-channel interference, where two subsystems operate on the same frequency and compete directly at the receiver, and adjacent channel interference, where signals from nearby frequency channels bleed into the target band, causing partial overlap and signal degradation [10]. The effects on the RF link include degradation of the carrier-to-noise ratio (CNR), increased bit error rate (BER), and reduction in link margin and throughput, which in severe cases leads to communication outages.

CubeSat platforms present a uniquely challenging environment for RFI management. The inherent SWaP constraints limit the physical separation between co-located RF subsystems, increasing the risk of near-field antenna coupling, structural chassis coupling, and frequency overlap between simultaneously operating links. Unlike larger satellite platforms where dedicated RF chains can be spatially isolated, CubeSat form factors force antenna placement on adjacent or orthogonal faces, with shared structural ground planes that can act as coupling paths between subsystems [11]. Effective RFI mitigation in multi-antenna satellite systems relies on a com-

The ALIGN project, led by Northumbria University, was funded by the UK Space Agency (UKSA) National Space Innovation Program (NSIP), grant UK–SAG22 0042, Phase 3 Implementation Stage of the project titled “ALIGN Laser Optical Communications for CubeSats.”, contract between 23 January 2023 and 31 March 2025.

bination of passive and active strategies, including physical separation, frequency planning, polarization diversity, filtering, and shielding [12]. For space applications with co-located antennas, orthogonal placement and polarization diversity are among the most practical passive isolation techniques, as they do not require additional hardware or mass. Dedicated bandpass filtering at the receiver input provides active out-of-band rejection, and is commonly integrated within modern CubeSat-qualified transceivers. Time Division Multiplexing (TDM) is an additional and widely adopted mitigation strategy, where co-located RF subsystems are scheduled to operate at different time slots, eliminating simultaneous transmission and effectively removing co-site interference at the protocol level.

For CubeSat platforms, TDM is particularly relevant as it simultaneously addresses RFI, power budget, and thermal constraints within a single protocol-level design decision, making it a mission-level requirement rather than purely an RF mitigation technique. On the other hand, the SWaP-C constraints impose significant limitations on the achievable isolation with hardware solution. Physical shielding between subsystems, while effective, adds mass and volume that may not be compatible with the CubeSat form factor, and is therefore treated as a design constraint rather than a baseline mitigation strategy.

University CubeSat projects face additional challenges. They suffer from budget limitations, particularly in the testing phase, to validate their design. Thus, in the early project phases, any solution must be addressed in the preliminary design based on standards and previous missions, and improved with lessons learned taking into account the existing mitigation techniques for the RF systems. This is consolidated by the idea that the projects are based on COTS hardware built and qualified for CubeSat. Although a comprehensive analysis of RFI mitigation is addressed in a future work, the validation approach adopted in this work is driven by these practical constraints typical of university CubeSat projects. In this context, the design relies on CubeSat-qualified COTS transceivers and antennas with inherent RF protections, providing confidence in its functional compatibility and suitability for space applications, complemented by mitigation techniques applied subject to SWaP constraints. Within these constraints, an end-to-end hardware demonstration feasibility using FM modules is presented in this work.

This paper is organized as follows: Section II describes the mission, the design constraints on the RF communication systems, and the proposed RFI mitigation mechanisms applied to the design. Section III details the test procedure, setup, and results. Section IV summarizes the conclusion with a presentation of future work.

II. System Under Test Description

A. Satellite Overview and RF Communication Systems Architecture

The ALIGN (Autonomous Laser-based Inter-satellite Gigabit Network) mission comprises a pair of 6U CubeSats equipped with FOCUS (Free-space Optical Communications Unit for Space), an experimental payload demonstrating high-data-rate optical inter-satellite links over a distance of 500–1000 km in sun-synchronous orbit (SSO). For associated papers connected to the FOCUS subsystems performance, see these papers [13]–[15]. The two satellites employ identical COTS-based designs with simplified interfaces to reduce the complexity and cost of the mission. Each satellite implements an electrical power subsystem (EPS), an attitude determination and control subsystem (ADCS), an onboard computer subsystem (OBC), as well as a dual RF communication subsystems. The latter comprises: the Radio Ground-to-Satellite Link (RGSL) for telemetry, tracking, and command (TT&C), and the Radio Inter-satellite Link (RISL) for direct satellite-to-satellite exchange, which is added as a support tool for the optical inter-satellite link to facilitate the pointing while reducing the pointing requirements on the ADCS. This dual RF configuration introduces a significant RFI management challenge inherent to the compact CubeSat form factor, addressed through the mitigation strategy presented in the following subsection. For more information see the manufacturer datasheet provided here[1].

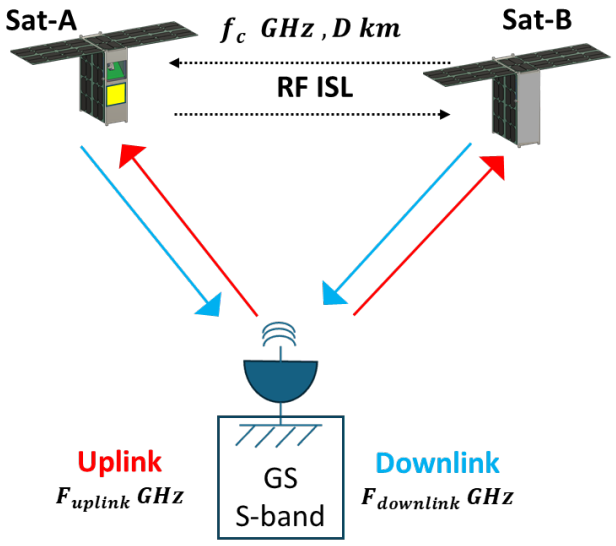

Fig. 1. Configuration of the dual RF communication links

B. Platform Design Constraint and Interference Risk Mitigation

For this project, the payload is the main driver of the mechanical and electrical design of the satellite; the objective is to fit the 6U platform form factor (100 x 226.3 x 366 mm). Although the internal module layout follows a straightforward split, allocating 3U to the payload and 3U to the platform modules, the external facet layout is more constrained. Each facet assignment is governed by the functional role of the hosted component, its performance requirements, and safety considerations relative to the 6U dispenser ejection system

[1]https://www.endurosat.com/

[16], significantly limiting the relocation options. The available external facets are shared among the solar panels, the payload aperture, Remove Before Flight (RBF) pins, S-band antennas, and ADCS sensors, the latter including magnetometers, sun sensors, a star tracker, and the GNSS antenna. The locations of the S-band antennas are specifically selected according to their dedicated functions. The RGSL antenna requires clear visibility towards the nadir axis for the ground link, while the RISL antenna requires clear visibility towards the inter-satellite link axis. Furthermore, both subsystems operate within the S-band frequency range (2025–2110 MHz) allocated by the International Telecommunication Union (ITU) for Earth-to-Space and Space-to-Space communication [17]. Consequently, the mitigation strategy implemented on the satellite combines different mechanisms, each addressing a specific aspect of the co-site RFI risk, as presented below.

1) TDM: In this mission, TDM is adopted as the primary mitigation strategy for nominal operations, as it simultaneously addresses RFI isolation, power budget, and thermal dissipation constraints within a single protocol-level design decision [16], [18]. However, hardware-level mitigation remains essential as a contingency, since simultaneous operation of the RGSL and RISL subsystems cannot be excluded in all mission scenarios, including commissioning, safe mode, and formation flying maneuvers where both ground and inter-satellite links must operate concurrently. Therefore, hardware-level mitigation strategies are implemented as a complementary layer of protection to ensure system integrity in all operational scenarios.

2) Transceivers specifications: The selected transceivers are compatible with the CubeSat standard and qualified for the space environment in accordance with the standards of ESA [19] and NASA GEVS [20]. To further consolidate the isolation strategy at the hardware level, the two transceivers are configured differently: the RGSL operates in full-duplex mode, while the RISL is configured for half-duplex operation. This asymmetric configuration provides an additional layer of hardware-level protection by ensuring that simultaneous transmission on both links is constrained by design, complementing the protocol-level TDM strategy described above. The RF front-end filtering of the selected transceivers is expected to contribute additional out-of-band rejection, complementing the passive isolation strategy, the characterization of which is planned as part of future qualification activities.

3) Frequency separation: Operating within the same allocated band introduces an inherent RFI risk for co-located antennas, including receiver desensitization effects when two RF systems operate at closely spaced frequencies [12], [21], [22]. To overcome this issue, for this initial configuration, a 55 MHz separation margin between the two distinct center frequencies of the respective systems (f_{c-RISL}= 2.030 GHz, f_{c-RGSL}= 2.085 GHz) is used, resulting in three distinct operating frequencies across the uplink, downlink, and inter-satellite link.

4) Spatial Isolation and Orthogonal Placement: The physical proximity of the two antennas within the 6U platform

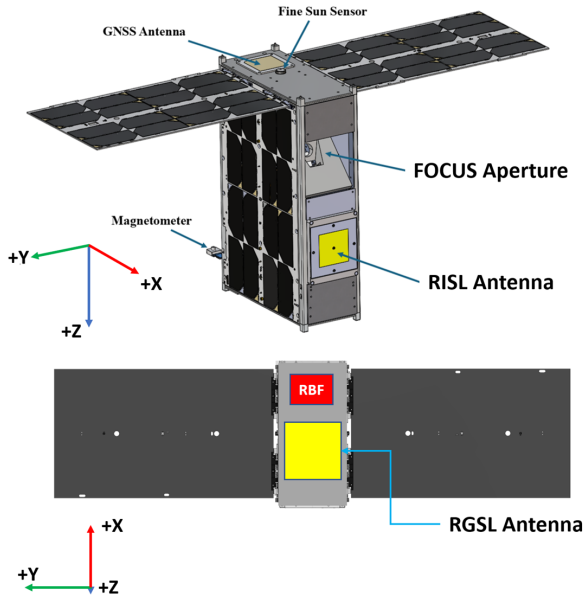

Fig. 2. ALIGN platform Dual antenna architecture

introduces co-site RFI challenges, which are addressed through orthogonal antenna placement [12], [22], [23]. Specifically, the RGSL patch antenna is positioned on the +Z nadir facet, providing clear visibility towards the nadir axis, while the RISL patch antenna is positioned on the +X forward facet co-located with the optical payload aperture to support the inter-satellite link geometry. This L-shape configuration achieves both physical separation and angular isolation between the two apertures, with a center-to-center distance of 15 cm and 90 ° angular isolation between boresight directions, as illustrated in Fig. 2. The 90 ° angular separation ensures that neither antenna operates within the main beam of the other, with both antennas seeing each other only at the θ = 90 ° edge of their respective radiation patterns, where the gain is significantly reduced relative to the boresight.

5) Polarization diversity: The RGSL employs Right-Hand Circular Polarization (RHCP), while the RISL operates with Linear Polarization (LP). RHCP is the predominant polarization convention for S-band satellite TT&C links, ensuring compatibility with ground segment infrastructure [12], [22]. The RISL antenna employs LP, which in combination with the RHCP of the RGSL provides inherent polarization diversity between the two links, contributing additional isolation as a passive RFI mitigation mechanism. Under ideal conditions, the polarization mismatch between RHCP and LP introduces a theoretical isolation of 3 dB, which may increase in practice depending on the relative antenna orientation [22], [23].

III. End-to-End System Demonstration

The aim of this test is to conduct a preliminary evaluation of the RFI environment between the RGSL and RISL subsystems operating simultaneously, identify any potential co-site interference, and establish initial confidence in the

Fig. 3. Antenna stand used for the test

implemented isolation strategy prior to formal qualification. This section presents the results of the RFI test conducted on the satellite COMM subsystems. The test was performed in a certified anechoic chamber at the Northumbria University facility, using FM modules of both the RGSL and RISL subsystems, together with a HackRF One Software Defined Radio (SDR) as an independent receiver for signal monitoring via waterfall diagram visualization.

A. Test Setup

The test setup was designed to replicate the mission's mechanical and electrical design parameters, ensuring that the antenna configuration remains consistent with the flight configuration (Fig. 3). The following conditions were maintained throughout the test:

- Two configurations were used to emulate the two satellites (A and B), each equipped with FM COMM modules
- Both transceivers were powered across their respective design-specified power levels and activated simultaneously
- Transmission was activated simultaneously where possible to identify any interference between the two links

A critical consideration in the test setup was ensuring that all measurements were performed under far-field conditions, which is a fundamental requirement for the results to be representative of the antenna radiation characteristics in a real propagation environment. The far-field boundary for both antennas was determined using the Fraunhofer criterion Eq.1 [23]:

$$d_f \geq \frac{2D^2}{\lambda} \tag{1}$$

where d_f is the far-field distance (m), D is the largest dimension of the antenna aperture (m), and λ is the free-space wavelength at the operating frequency (m), calculated as $\lambda = c/f_c$, where c is the speed of light (m/s), and f_c is the center frequency (Hz).

Both RGSL and RISL antennas are designed to fit within a 1U face (100 × 100 mm), giving a diagonal aperture dimension of D ≈ 141.4 mm. At their respective selected center frequencies of 2.085 GHz and 2.030 GHz, the corresponding free-space wavelengths are λ_A = 14.4 cm and λ_B = 14.8 cm, producing far-field distances of approximately d_{fA} = 27.8 cm and d_{fB} = 27.1 cm respectively. The test was conducted at a fixed separation distance of 2 m between the transmitting and receiving antennas, satisfying the far-field condition by a factor of approximately 7 for both links, ensuring that the measured signal levels and isolation performance are representative of far-field propagation behavior.

The transceivers were monitored and controlled using the manufacturer's dedicated Assembly, Integration, and Test (AIT) software[2], enabling full configuration control of key RF parameters including operating frequency, transmit power, modulation type, satellite ID, and temperature, among others. Packet transmission and reception were managed through the same interface, allowing the number of transmitted packets to be verified against those received at the other end. Both single and successive packet transmissions were used to distinguish individual link events between Sat-A and Sat-B in both directions. Simultaneously, the HackRF One SDR waterfall diagram provided independent visual confirmation of signal presence and frequency occupancy for each active link.

Transmit power levels from 26 dBm to 33 dBm were evaluated to cover the full operational range of each link as defined by the mission power budget, spanning from the nominal operational power up to the maximum allowed transmit power. This approach ensures that the interference assessment reflects both nominal and worst-case operational conditions, with the maximum transmit power of 33 dBm representing the most demanding scenario in terms of potential co-site RFI towards the RGSL.

While a formal conducted isolation measurement, such as the S_{21} parameter between the two antenna ports using a vector network analyzer (VNA), represents the conventional characterization method, such equipment is not always accessible within the resource and budget constraints typical of university CubeSat projects. In this context, a functional radiated test in a controlled anechoic environment constitutes a valid and meaningful first-step validation approach, capable of demonstrating the absence of interference between the two RF links under realistic operational conditions. The overall test configuration is illustrated in Fig. 4.

B. Test Procedure

The test was conducted in two phases. The first phase used the HackRF One SDR as a receiver for handshake confirmation. The objective of this phase was to verify that all modules operate correctly and transmit signals as expected. Different frequencies were assigned to each module so that individual signals could be distinguished on the waterfall diagram upon reception. The test sequence was as follows:

1) Independent transmission from each module with signal reception confirmed at the SDR
2) Handshake and link establishment between the SDR and RGSL, and between the two RISL modules
3) Interference test between the RGSL and RISL modules operating simultaneously

[2]https://www.endurosat.com/spacedev/

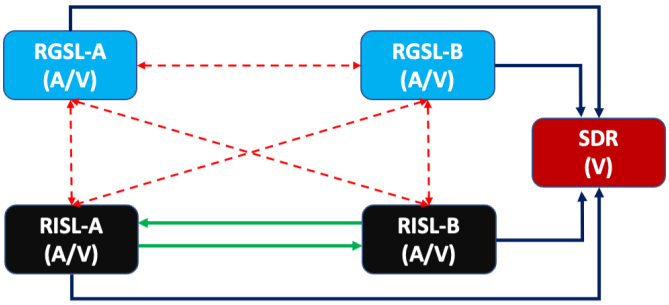

Fig. 4. Dual S-band RF link test configuration for co-site RFI assessment. A: Aggressor, V: Victim. Green arrows indicate successful bilateral ISL links, red dashed arrows indicate absence of co-site RFI at RGSL receivers, and blue arrows indicate S-band signal detection at the SDR

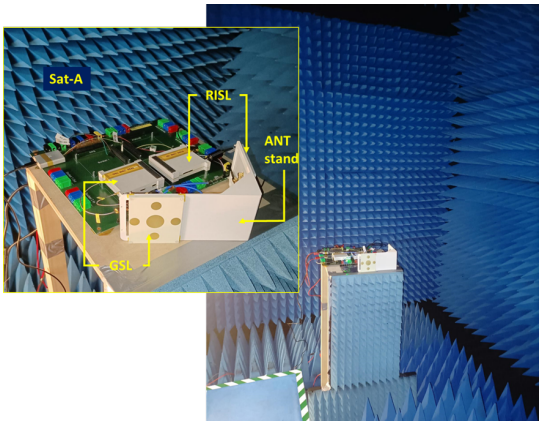

Fig. 5. FlatSats mockup setup in the anechoic chamber

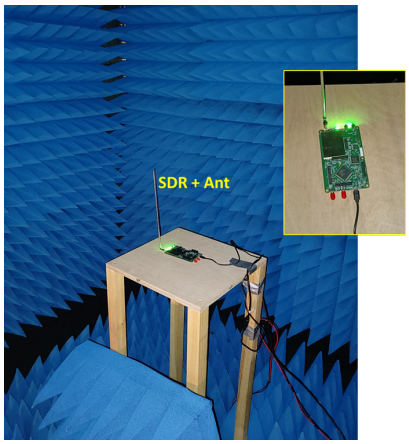

Fig. 6. SDR setup in the anechoic chamber

In the second phase, the objective was to confirm the inter-satellite handshake performance under realistic interference conditions. In this configuration, the two RISL modules acted as aggressors, while RGSL and SDR served as victims. Following the same transmit/receive protocol, the test was conducted bilaterally.

In the first configuration, RISL-A transmitted while the received signal was monitored at RISL-B, RGSL-A/B, and the SDR. The roles were then reversed, with RISL-B transmitting and the received signal monitored at RISL-A, RGSL-A/B, and the SDR. Throughout both configurations, different transmit power levels and antenna orientations were evaluated to assess isolation performance across the entire operational envelope.

It should be noted that RGSL transceivers require dedicated ground station emulation software to establish a link, which was unavailable due to budget constraints. However, this limitation was leveraged as a detection advantage: any packet received at the RGSL during transmission would constitute unambiguous evidence of co-site RFI. The absence of any such reception across all configurations therefore provides a direct and conservative validation of the isolation strategy, reflected in the results table where the RGSL receiver entries are marked NA (Not Applicable).

C. Results and Discussion

The results, summarized in Table II, confirmed successful operation across all test configurations. The absence of interference observed across all power levels and antenna orientations can be attributed to the combined effect of isolation mechanisms implemented in the dual RF architecture. First, the orthogonal antenna placement, with the RGSL patch antenna on the +Z nadir face and the RISL patch antenna on the +X forward face, provides a fixed physical separation of 15 cm and 90° angular isolation between the two apertures. Second, the inherent polarization diversity between the two links contributes an additional isolation margin, as the RGSL employs Right-Hand Circular Polarization (RHCP) while the RISL operates with Linear Polarization (LP), providing 3 dB of additional isolation [22], [23]. Third, the separate and non-overlapping frequency assignments for the RGSL and RISL links ensure that co-channel interference is avoided by design.

These results demonstrate that the dual RF architecture achieves sufficient isolation between the RGSL and RISL links under far-field conditions and across the full operational power range, validating the orthogonal antenna placement strategy as an effective and practical approach to co-site RFI mitigation within the SWaP-C constraints of a 6U CubeSat platform. Thermal and conducted isolation validation are planned as part of the subsequent qualification campaign.

IV. SUMMARY AND CONCLUSIONS

This paper presented the RF communication system architecture and end-to-end RFI preliminary feasibility demonstration for the ALIGN mission, a dual 6U CubeSat platform featuring co-located S-band RGSL and RISL subsystems. A multi-layered mitigation strategy was implemented, combining TDM at the protocol level with hardware-level isolation strategies including asymmetric transceiver duplex configuration, 55 MHz frequency separation, orthogonal antenna placement providing 15 cm physical separation and 90° angular isolation, and polarization diversity between the RHCP RGSL and LP RISL links providing a theoretical isolation of 3 dB.

TABLE I
MONITORED RF PARAMETERS AND TELEMETRY DATA
FOR THE MODULES DURING THE TEST

Parameter	RGSL	RISL-A	RISL-B
Power Configuration			
Target Power ± 1 (dBm)	26	31	26
Packet Counters			
Transmitted Packets	19	3	2
Received Packets	0	2	3
Temperatures			
MCU Temperature ($\pm 0.1^{\circ}$C)	31	30	29.5
PA Temperature ($\pm 0.1^{\circ}$C)	29.92	28.48	28.48
Transmit Data			
Type (Exact)	AUTO (0x01)	AUTO (0x01)	AUTO (0x01)
Payload (ASCII)	"hello"	"hello"	"hello"

TABLE II
END-TO-END RF INTERFERENCE TEST RESULTS
(P/F STAND FOR P: TEST PASSED, F: TEST FAILED)

Receiver	Transmitter				Requirement	P/F
	RGSL-A	RISL-A	RGSL-B	RISL-B		
RGSL-A	X	X	**NA**	X	Receive only the signal from similar transmitter	**P**
RISL-A	X	X	X	✓	Receive only the signal from similar transmitter	**P**
RGSL-B	**NA**	X	X	X	Receive only the signal from similar transmitter	**P**
RISL-B	X	✓	X	X	Receive only the signal from similar transmitter	**P**
SDR	✓	✓	✓	✓	Receive any signal in the frequency range specified	**P**

The end-to-end hardware feasibility test was conducted using FM modules in a certified anechoic chamber under far-field conditions and across the full operational power range of both links. The results confirmed successful bilateral RISL handshake and the absence of co-site RFI at the RGSL across all tested configurations, validating the combined isolation strategy as an effective and practical approach within the SWaP constraints of a 6U CubeSat platform.

Future work will investigate the effect of reduced and identical center frequency configurations on mission RF performance, informing design changes prior to the Critical Design Review (CDR). This will be complemented by conducted isolation measurements using a VNA to formally quantify antenna port isolation, and thermal validation of RF communication system performance through TVAC qualification testing, as part of the pre-CDR design consolidation and formal qualification campaign.

ACKNOWLEDGMENT

The authors would like to pay special thanks to project partners Telespazio UK Ltd, CfAI Durham University, and SMS Electronics Ltd for continued support throughout the project period.

REFERENCES

[1] K.-P. Bouzoukis, G. Moraitis, V. Kostopoulos, and V. Lappas, "An Overview of CubeSat Missions and Applications," *Aerospace*, vol. 12, no. 6, p. 550, Jun. 2025, publisher: Multidisciplinary Digital Publishing Institute. [Online]. Available: https://www.mdpi.com/2226-4310/12/6/550

[2] P. Shafiei, J. Bemtgen, and S. Tabibi, "Precise orbit determination of Spire CubeSats constellation using the raw observation approach," *Advances in Space Research*, vol. 76, no. 5, pp. 3122–3141, Sep. 2025. [Online]. Available: https://linkinghub.elsevier.com/retrieve/pii/S0273117725006544

[3] J. Crusan and C. Galica, "NASA's CubeSat Launch Initiative: Enabling broad access to space," *Acta Astronautica*, vol. 157, pp. 51–60, Apr. 2019. [Online]. Available: https://linkinghub.elsevier.com/retrieve/pii/S0094576517303107

[4] [Online]. Available: https://digitalcommons.usu.edu/cgi/viewcontent.cgi?article=4108&context=smallsat

[5] J. D. Monnier, P. Jain, S. Kalluri, J. Cutler, S. D'Amico, G. Lightsey, L. Pogorelyuk, G. Vasisht, K. Cahoy, and M. Meyer, "STARI: starlight acquisition and reflection toward interferometry," in *Space Telescopes and Instrumentation 2024: Optical, Infrared, and Millimeter Wave*, L. E. Coyle, M. D. Perrin, and S. Matsuura, Eds. Yokohama, Japan: SPIE, Aug. 2024, p. 112. [Online]. Available: https://www.spiedigitallibrary.org/conference-proceedings-of-spie/13092/3020785/STARI-starlight-acquisition-and-reflection-toward-interferometry/10.1117/12.3020785.full

[6] J. Guo, P. Hoogeboom, P. L. Dekker, J. Bouwmeester, G. Meoni, J. Nieto, J. Fayos, E. Bertels, and C. Pirat, "AltiCube+: A low-cost long fixed-baseline radar altimeter solution based on cubesats on-orbit assembly," *Acta Astronautica*, vol. 235, pp. 584–595, Oct.

2025. [Online]. Available: https://linkinghub.elsevier.com/retrieve/pii/S0094576525003376

[7] "Ariane 6 launches: NASA's radio detective CURIE." [Online]. Available: https://www.esa.int/Enabling_Support/Space_Transportation/Ariane/Ariane_6_launches_NASA_s_radio_detective_CURIE

[8] M. Silver, A. Lopez, D. Howe, E. Thompson, A. Morris, A. Fenn, M. Knapp, P. Erickson, F. Lind, L. Paritsky, R. Masterson, K. Ammons, N. Belsten, E. Kononov, and C. Payne, "Development of the Deployable HF Vector Sensor for the AERO-VISTA Spacecraft," in *2024 IEEE Aerospace Conference*, Mar. 2024, pp. 1–10, iSSN: 1095-323X. [Online]. Available: https://ieeexplore.ieee.org/abstract/document/10521397

[9] J. T. Johnson, C. Ball, C.-C. Chen, C. McKelvey, G. E. Smith, M. Andrews, A. O'Brien, J. L. Garry, S. Misra, R. Bendig, C. Felten, S. Brown, R. F. Jarnot, J. Kocz, K. Horgan, J. F. Lucey, J. J. Knuble, M. Solly, C. Duran-Aviles, J. Peng, D. Bradley, J. R. Piepmeier, D. Laczkowski, M. Pallas, N. Monahan, and E. Krauss, "Real-Time Detection and Filtering of Radio Frequency Interference Onboard a Spaceborne Microwave Radiometer: The CubeRRT Mission," *IEEE Journal of Selected Topics in Applied Earth Observations and Remote Sensing*, vol. 13, pp. 1610–1624, 2020. [Online]. Available: https://ieeexplore.ieee.org/document/9061029/

[10] E. Kang, J. Yang, Y. Park, J. Kim, W. Shin, Y. B. Park, and H. Choo, "Analysis of a Low-Earth Orbit Satellite Downlink Considering Antenna Radiation Patterns and Space Environment in Interference Situations," *Remote Sensing*, vol. 15, no. 7, p. 1748, Mar. 2023. [Online]. Available: https://www.mdpi.com/2072-4292/15/7/1748

[11] A. Zeedan and T. Khattab, "CubeSat Communication Subsystems: A Review of On-Board Transceiver Architectures, Protocols, and Performance," *IEEE Access*, vol. 11, pp. 88 161–88 183, 2023. [Online]. Available: https://ieeexplore.ieee.org/document/10224067/

[12] *Space Antenna Handbook*, William a. imbriale, steven (shichang) gao, luigi boccia ed., May 2012.

[13] C. Graham, D. Bramall, O. Younus, A. Riaz, R. Binns, E. Scullion, R. T. Wicks, and C. Bourgenot, "Steering Mirror System with Closed-Loop Feedback for Free-Space Optical Communication Terminals," *Aerospace*, vol. 11, no. 5, p. 330, May 2024, publisher: Multidisciplinary Digital Publishing Institute. [Online]. Available: https://www.mdpi.com/2226-4310/11/5/330

[14] O. I. Younus, A. Riaz, R. Binns, E. Scullion, R. Wicks, J. Vernon, C. Graham, D. Bramall, J. Schmoll, and C. Bourgenot, "Overview of Space-Based Laser Communication Missions and Payloads: Insights from the Autonomous Laser Inter-Satellite Gigabit Network (ALIGN)," *Aerospace*, vol. 11, no. 11, p. 907, Nov. 2024, publisher: Multidisciplinary Digital Publishing Institute. [Online]. Available: https://www.mdpi.com/2226-4310/11/11/907

[15] A. Riaz, E. Scullion, R. Wicks, Z. Ahmed, E. Obreque, N. Khorchef, J. Vernon, C. Del Valle, R. Zia-ul Mustafa, R. Binns, and J. Martin, "Characterisation of amplified laser beam profiles subject to changing EDFA pump currents in CubeSats," in *Free-Space Laser Communications XXXVIII*, H. Hemmati and B. S. Robinson, Eds. San Francisco, United States: SPIE, Mar. 2026, p. 64. [Online]. Available: https://www.spiedigitallibrary.org/conference-proceedings-of-spie/13885/3091804/Characterisation-of-amplified-laser-beam-profiles-subject-to-changing-EDFA/10.1117/12.3091804.full

[16] C. Cal Poly – San Luis Obispo, "CubeSat Design Specification (1U – 12U)," Feb. 2022. [Online]. Available: https://static1.squarespace.com/static/5418c831e4b0fa4ecac1bacd/t/62193b7fc9e72e0053f00910/1645820809779/CDS+REV14_1+2022-02-09.pdf

[17] I. T. U. ITU, "Radio Regulations Articles," Tech. Rep., 2020. [Online]. Available: https://www.itu.int/en/ITU-R/seminars/rrs/RRS-23-Africa/Presentations/ITU-R%20Regulatory%20Documents/1.Radio%20Regulations%20and%20Rules%20of%20Procedure/Radio%20Regulations%20Ed%202020_WRC-19/Radio%20Regulations%20Ed%202020-English/RR-2020-Vol%201_E.pdf

[18] A. Zeedan and T. Khattab, "A Critical Review of Baseband Architectures for CubeSats' Communication Systems." [Online]. Available: https://www.authorea.com/doi/full/10.36227/techrxiv.18982553.v1?commit=7a10883469543c6d18539980f9f99760e73ac146

[19] "Space engineering _testing," May 2022. [Online]. Available: https://ecss.nl/wp-content/uploads/2022/05/ECSS-E-ST-10-03-Rev.1(31May2022).pdf

[20] "GENERAL ENVIRONMENTAL VERIFICATION STANDARD (GEVS) For GSFC Flight Programs and Projects." [Online]. Available: https://soma.larc.nasa.gov/lws/pdf_files/3.12%20GSFC-STD-7000A.pdf

[21] A. Lovascio, A. D'Orazio, and V. Centonze, "Characterization of a COTS-Based RF Receiver for Cubesat Applications," *Sensors*, vol. 20, no. 3, p. 776, Jan. 2020, publisher: Multidisciplinary Digital Publishing Institute. [Online]. Available: https://www.mdpi.com/1424-8220/20/3/776

[22] G. Maral and M. Bousquet, *Satellite Communications Systems: Systems, Techniques and Technology*. John Wiley & Sons, Aug. 2011, google-Books-ID: PEsmLaDXzvsC.

[23] C. A. Balanis, *Antenna Theory: Analysis and Design*. John Wiley & Sons, Feb. 2016, google-Books-ID: iFEBCgAAQBAJ.